JACS
JOURNAL OF THE AMERICAN CHEMICAL SOCIETY

Article

pubs.acs.org/JACS

Quantification of Fewer than Ten Copies of a DNA Biomarker without Amplification or Labeling

Yoonhee Lee,[†] Youngkyu Kim,[†] Donggyu Lee,[‡] Dhruvajyoti Roy,[§] and Joon Won Park*[,†,‡]

[†]Department of Chemistry, and [‡]Division of Integrative Biosciences and Biotechnology, Pohang University of Science and Technology, 77 Cheongam-Ro, Nam-Gu, Pohang 37673, Republic of Korea

[§]Nanogea Inc., 6162 Bristol Parkway, Culver City, California 90230, United States

Supporting Information

ABSTRACT: Polymerase chain reaction (PCR) is a highly sensitive diagnosis technique for detection of nucleic acids and for monitoring residual disease; however, PCR can be unreliable for samples containing very few target molecules. Here, we describe a quantification method, using force−distance (FD) curve based atomic force microscopy (AFM) to detect a target DNA bound to small (1.4−1.9 μm diameter) probe DNA spots, allowing mapping of entire spots to nanometer resolution. Using a synthetic *BCR-ABL* fusion gene sequence target, we examined samples containing between one and 10 target copies. A high degree of correlation (r^2 = 0.994) between numbers of target copies and detected probe clusters was observed, and the approach could detect the *BCR-ABL* biomarker when only a single copy was present, although multiple screens were required. Our results clearly demonstrate that FD curve-based imaging is suitable for quantitative analysis of fewer than 10 copies of DNA biomarkers without amplification, modification, or labeling.

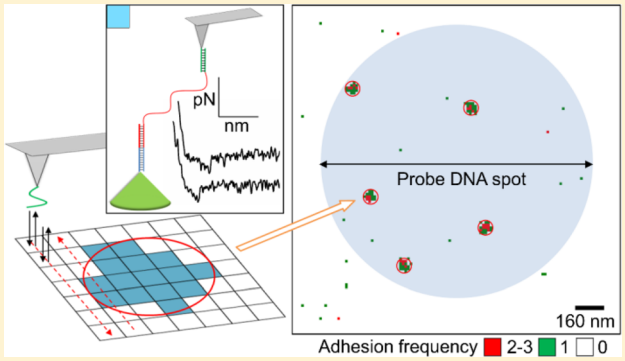

INTRODUCTION

Biomarkers have emerged as useful tools in oncology, facilitating early diagnosis and disease surveillance during therapy. Quantification techniques designed to enhance limits of detection (LOD) have become essential to track residual disease, determine when therapy is complete and decrease the risk of relapse. Real-time quantitative polymerase chain reaction (qPCR) has played a key role as a sensitive tool in molecular biology and diagnostics.[1−3] This technique allows precise quantification of nucleic acids by recording fluorescence intensity correlated with their exponential PCR amplification. Targets are quantified by comparison with an amplification curve from a standard material; however, the method is not suitable for the quantification of genes expressed at a low level (<10 copies/sample), since false positive results can occur as a result of amplification errors, such as primer-dimers.[4,5] In addition, the efficiency of amplification relies on nucleic acid structure, and errors in calibration of the target and standard material are also a source of uncertainty in this approach.[6] Digital PCR is a newly developed alternative technique that overcomes dependency on standard materials.[7−9] Individual targets are statistically distributed in partitions or droplets and amplified in parallel, and the target concentration is determined by counting positive partitions after PCR completion. However, the partition volume is a key factor in determining the number of targets, and errors in estimating and controlling volume can generate nontrivial bias in absolute quantification.[10]

Therefore, technological developments in molecular diagnostics have focused on sensitive assays using nanopores, nanoparticles, and molecular beacons for amplification-free quantification.[11−13] Moreover, state-of-the-art technologies for single molecule visualization, such as single molecule fluorescence microscopy and single molecule force spectroscopy, have been investigated as diagnostic tools.

In this study, we used atomic force microscopy (AFM) for direct and sensitive quantification of a DNA biomarker present at extremely low copy numbers. AFM has been applied to study DNA−DNA, ligand−receptor, and RNA−protein interactions by monitoring the adhesion force between a probe tethered to an AFM tip and a target coated in the substrate. In particular, AFM is well-established as a tool for investigation of the biomolecular interactions involved in DNA hybridization.[14,15] The rupture of the DNA duplex under various pulling geometries, such as unzipping and shearing, has been precisely analyzed, and the forces required in respect of oligonucleotide length have been quantitatively resolved.[16] An important mode of AFM is force−distance (FD) curve-based imaging, which generates a map of FD curves over sample surfaces.[17] It enables localization of molecular interactions on the surface at nanometer resolution, and several biological assays have been reported, including the quantification of a specific mRNA, and the measurement of Young's modulus on cancer cell

Received: March 16, 2016
Published: May 13, 2016

DOI: 10.1021/jacs.6b02791
J. Am. Chem. Soc. 2016, 138, 7075−7081

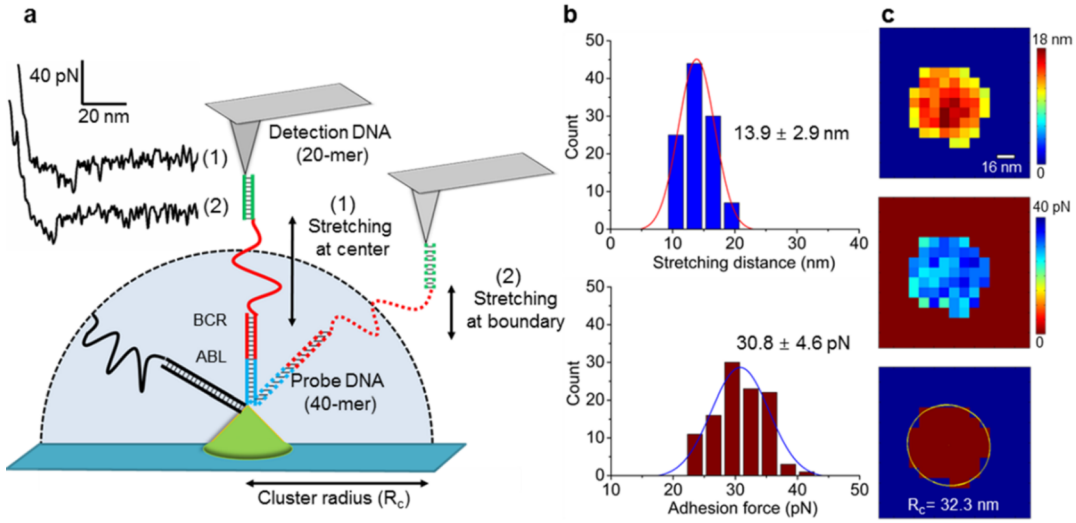

Figure 1. Localization of a single target DNA species by adhesion force mapping. (a) Measurement of the cluster radius of a captured target DNA by detection of DNA binding between the tip and the substrate. A cluster of specific pixels was observed when the AFM tip examined positions with 8.0 nm separation, and variation of FD curve characteristics was observed within clusters according to pulling angle. (b) Histograms of stretching distance (top) and adhesion force values (bottom) measured from FD curves (n = 102). (c) Stretching distance map (top), adhesion force map (middle), and ellipse fitting image of a representative cluster (bottom).

surfaces.[18,19] Recent developments in AFM technology open a new way to obtain a force map and directly correlate it with a topographic image of a surface within a reasonable time frame. Further progress will likely enable the adoption of AFM in the field of molecular diagnostics in the future.[20−22]

FD curve-based DNA assays of very low copy number targets must scan the whole surface containing the target DNAs. In this context, we fabricated a small probe DNA spot, with a diameter <2.0 μm, for nanometer-resolution imaging using AFM. As proof of concept, we used a synthetic *BCR-ABL* sequence (a biomarker of chronic myeloid leukemia; CML),[23,24] and characterized a FD curve-based DNA assay for this biomarker when fewer than ten copies were present.

RESULTS

Mapping the Hydrodynamic Radius of a Single Target DNA Molecule and Spotting of Probe DNA. FD curves were collected pixel by pixel from a probe DNA spot, and the AFM tip could only recognize captured target DNA when the tip entered the volume defined by its hydrodynamic radius (Figure 1a). Therefore, measurement of the hydrodynamic radius of the target DNA is the first step in determining the optimal pixel size; if pixels are too small, mapping of a specific area will take more time, and, if pixels are too large, AFM may miss the captured DNA or the captured DNA may be detected as a single pixel. In the latter case, it becomes difficult to differentiate specific pixels from randomly distributed non-specific pixels. The DNA probe (40-mer) was designed to specifically bind to the junction region of the *BCR-ABL* gene (Figure S1 in the Supporting Information). The detection DNA (20-mer), which was designed to hybridize to the *BCR* region of the target DNA, was attached to the apex of an AFM tip. When the probe DNA captured the target, the target DNA was stretched using the AFM tip until rupture of the shorter duplex occurred. Adhesion force maps for the isolated single target DNA molecule were obtained with a pixel size of 8.0 nm. Characteristic FD curves showing molecular stretching were detected in the map, and the most probable stretching distance was 13.9 ± 2.9 nm with an adhesion force of 30.8 ± 4.6 pN (Figure 1b). The pixels exhibiting specific adhesions are presented in Figure 1c, and are assembled in a circular area indicating a tethered DNA motion. We performed a control experiment to evaluate the reliability of the interaction by adding a free DNA that can block the hybridization sites of the AFM tip. Characteristic adhesions were rarely observed after blocking, and clusters were not observed (Figure S2 in the Supporting Information).

The cluster radius (R_c) was measured by ellipse fitting to estimate the hydrodynamic radius of the target DNA,[25] and a small amount of drift rendered the cluster almost circular. Three or six force maps were collected from each location, and three consecutive maps were superimposed to obtain one or two overlaid maps per location; a total of five overlaid maps were obtained from three different locations. The average cluster radius of the overlaid maps was 29.9 ± 4.2 nm. The concentric contour of the stretching distance was determined for each cluster (Figure 1c); the features of this were determined by the pulling angle between the AFM tip and the target. Maximum extension was observed at the center of a cluster, demonstrating that a bound target DNA molecule (a single strand of 110-mer) could be stretched by up to 30% of its contour length (unit length = 0.59 nm).[26]

Simulation studies demonstrated that there are two main hairpin loops in the *BCR-ABL* sequence used in this study (Figure S3 in the Supporting Information).[27,28] Discrepancy between the observed stretching length and the contour length can occur where the effective pulling force applied to the target DNA is not sufficiently large to permit stretching to almost its full contour length. In comparison with the observed stretching distance values, the cluster radius of the target DNA was longer. This is explained by the fact that the duplex generated by the probe and the target DNA hybridization (40 bp) contributes to the hydrodynamic radius. The duplex is expected to behave as a free-moving rigid rod.[29]

From these observations, we were able to determine the optimized pixel size of the probe DNA spot for the visualization of individual targets. Using a scan speed of 0.25 s/pixel, the examination of 128 × 128 pixels takes 70 min. When 128 × 128

DOI: 10.1021/jacs.6b02791
J. Am. Chem. Soc. 2016, 138, 7075−7081

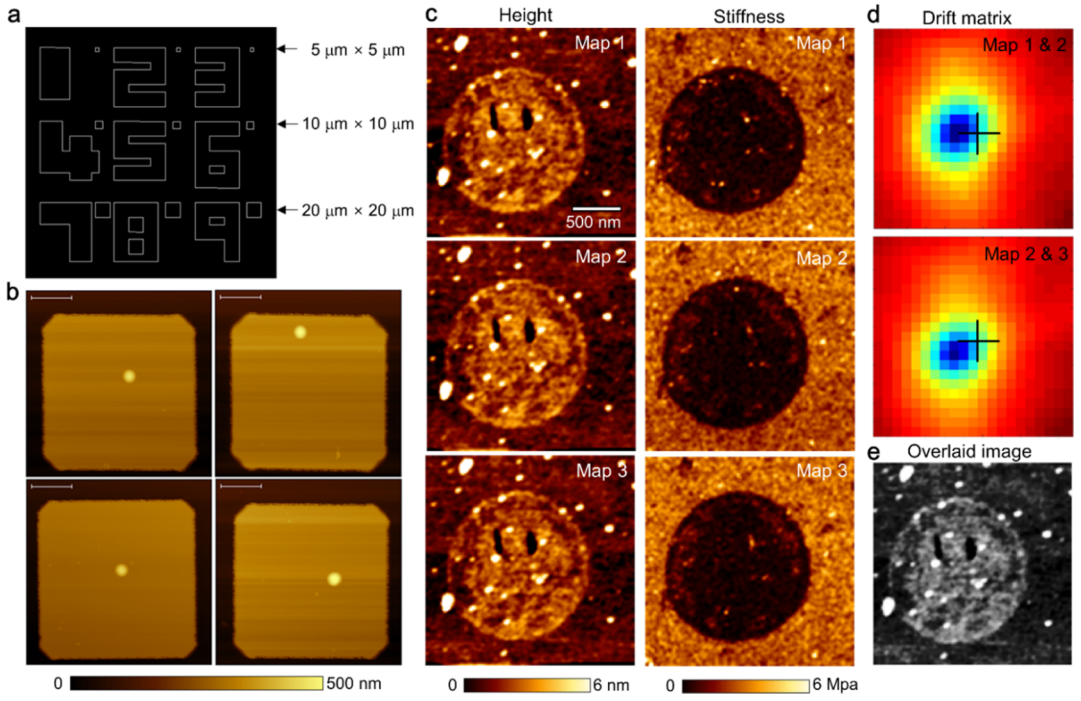

Figure 2. Probe DNA spot fabrication using FluidFM and calculation of the lateral drift from spot images. (a) Schematic diagram of the etched slide glass. (b) AFM topographic images of the DNA spots within the etched square boxes (20 × 20 μm^2). The precise position of each spot with respect to a point at the edge of the box was recorded (scale bar = 5 μm). (c) Three consecutively obtained height images of a spot (128 × 128 pixels) and corresponding Young's modulus images exported from the slope images. (d) A program created in-house was used to determine the drift between the maps. For the example shown, height images were used for the calculation. The program demonstrated that the difference between the maps was minimal by moving one of the maps to the point indicated by the center of the blue pixels. The required offset in the *x* and *y* axes was calculated from the center of the blue pixels and the center of the map (marked by +). The drift offset was (−2,0) between the first and second maps, and (−2,−2) between the second and third maps. (e) The final map was obtained when the first map was overlaid onto the second, and the third map was overlaid onto the fused first and second maps.

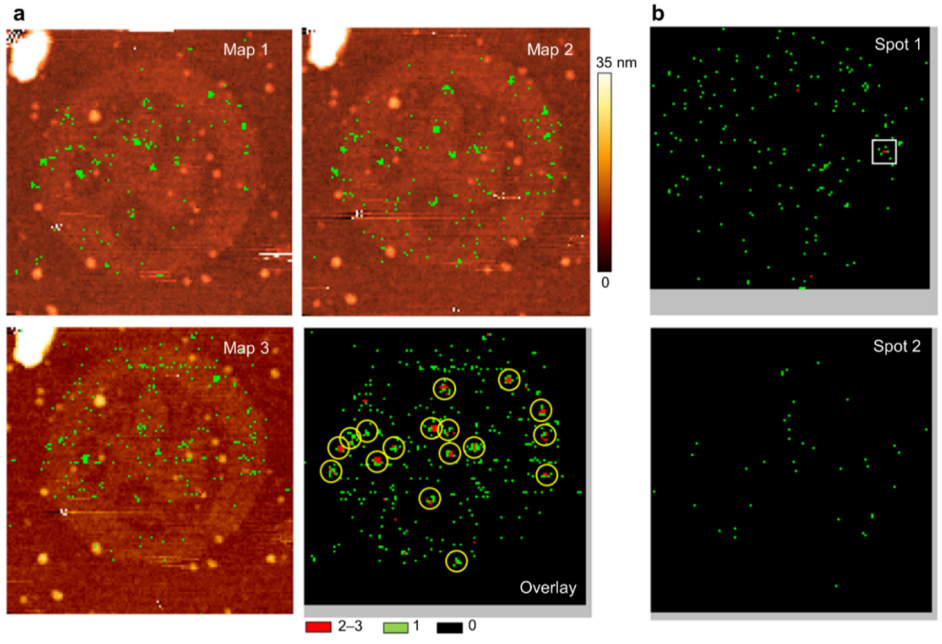

Figure 3. Superimposing specific adhesion maps. (a) Three consecutive adhesion maps (128 × 128 pixels, 2.25 × 2.25 μm^2) after hybridization with *BCR-ABL* gene sequence (1.0 aM, 40 μL). These maps were merged after correcting for drift. The pixels where a single specific FD curve was collected are colored green. Pixels where two or three specific FD curves were collected are colored red. Some sections were not overlaid; these are colored gray. Yellow circles indicate the locations where repeated detection was observed and the cluster size qualified as positive ($R_c \geq 26$ nm). (b) Two overlaid adhesion force maps in the absence of exposure to target DNA. The largest cluster (white square box, R_c = 25.2 nm) was observed in one spot among the nine spots examined.

DOI: 10.1021/jacs.6b02791
J. Am. Chem. Soc. 2016, 138, 7075−7081

Table 1. Number of Clusters Observed in Each Probe DNA Spot at Various Concentrations of Target

		observed number of clusters ($R_c \geq 26.0$ nm) in a spot										
sample (zM)	theoretical copy numbers	spot 1	spot 2	spot 3	spot 4	spot 5	spot 6	spot 7	spot 8	spot 9	mean	SD
0	0	0	0	0	0	0	0	0	0	0		
40	1	0	0	0	1	0	0	0	0	1	0.22	0.44
80	2	1	0	0	2	0					0.60	0.89
200	5	3	2	2	3	2					2.40	0.55
400	10	6	3	5							4.67	1.53

pixels are examined on the probe DNA spot with a 2.0 μm diameter, the pixel size is 15.6 nm, which is sufficiently small to observe a cluster of pixels representing each specific target DNA in the map. In practice, an area slightly larger than the spot was scanned to examine the entire area of a spot by increasing the pixel size up to 18.4 nm.

We employed FluidFM technology for the fabrication of probe DNA spots < 2.0 μm. This technology uses a cantilever, with a closed channel connecting the tip opening to a fluid reservoir.[30] The microchannel was filled with probe DNA solution, and the solution was delivered onto a glass surface activated with *N*-hydroxysuccinimide (NHS). To effectively detect the tiny spot using AFM, it was necessary to spot the probe DNA at a position with known x, y coordinates. To this end, photolithographic etching was performed to mark out multiple micron size square boxes on the slide (Figure 2a). Probe DNA was spotted on a predefined position within the square boxes (20×20 μm^2), and the average spot diameter was observed to be 1.48 ± 0.06 μm (Figure 2b). While the within-batch variation was quite narrow, different batches produced spots of diameters varying between 1.4 and 1.9 μm.

Drift-Corrected Overlay of Adhesion Force Maps and Cluster-Counting Criteria. To improve reliability, we collected three force maps consecutively and overlaid them.[22] In the AFM force mapping mode, we simultaneously recorded piezo movement in the *z*-direction (height), degree of cantilever bending (slope), and the maximum force of retraction in the FD curve (adhesion), and converted the data into three characteristic images. Using the height or slope images (Figure 2c), we measured the lateral drift (measured in pixels) between the first two, and last two images using in-house software (Figure 2d and e). FD curves for the individual adhesion maps were filtered to leave those showing the specific stretching distance (10−40 nm) and appropriate adhesion force value (≤40 pN). For positive pixels, where specific FD curves were recorded, two-dimensional images were then generated. Three specific adhesion maps were then overlaid after correcting for drift. In the overlaid specific adhesion map, pixels where two or three specific curves were detected are colored in red, and pixels with a single specific event are colored in green. Given the high event probability at the center of the clusters, red pixels are evident in maps obtained from exposure to the target DNA (1.0 aM, 40 μL) (Figure 3a). As a negative control, we examined nine spots without target DNA, and found that red colored pixels were rarely observed (Figure 3b). In addition, the majority of clusters were small, with the radius of the largest cluster among the nine negative control overlaid maps being 25.2 nm. Based on the observation, we set out the following rules to assign the positive clusters: (1) a cluster must have no less than one pixel showing repetitive adhesion events; (2) a cluster must be over 26.0 nm in radius. Using these criteria, 17 clusters qualified as positive in the sample described (Figure 3a). The average cluster radius was 36.9 ± 6.6 nm, and the average number of pixels in the cluster (defined as 87% occupancy within the fitted area) was 10.4 ± 3.2. The above criteria were used consistently for the analysis of further samples.

Analysis of Samples Containing Fewer than Ten Copies of Target DNA. The target DNA was serially diluted to make solutions of 4.0×10^1 zM (40 μL, one copy), 8.0×10^1 zM (40 μL, two copies), 2.0×10^2 zM (40 μL, five copies), and 4.0×10^2 zM (40 μL, ten copies), and each solution was applied to a probe DNA spot. Hybridization was performed at 52 °C for 24 h to ensure effective capture of targets. To account for sample preparation error, capture efficiency, detection efficiency, and other factors influencing quantification, multiple replicate experiments were carried out using independent samples. For the single copy sample, nine replicates were performed, and, for samples with higher copy numbers, three or five replicates were performed (Table 1). Positive clusters meeting the criteria outlined above (i.e., radius ≥ 26.0 nm) were counted, and the average number of clusters was plotted with respect to target copy number (Figure 4a). For samples

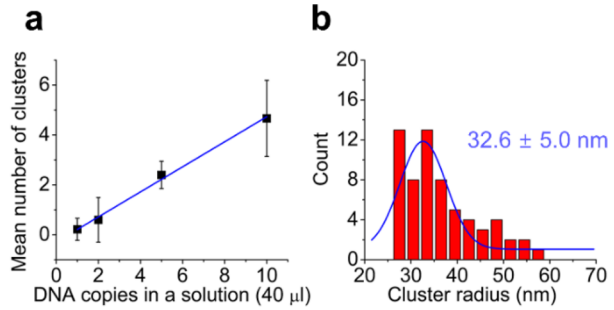

Figure 4. Quantification of target DNA consisting of fewer than ten copies. (a) Plot showing the correlation between the average cluster number and the copy number in solution. The data were fitted linearly, and the slope was 0.50 with an adjusted R^2 value of 0.994. (b) Histogram of the measured cluster radii (n = 63).

with a single copy, a single cluster was detected twice among the nine replicate experiments. For samples with two copies, a single cluster or two clusters were detected in two of the five replicate experiments. For samples with five and ten copies, clusters were observed in all replicate experiments, with the average numbers of clusters detected being 2.40 and 4.67, respectively. There was a strong linear correlation between cluster number and copy number (adjusted R^2 of 0.994, linear regression model). The detection efficiencies were respectively 48% and 47% for samples containing five and ten copies of target DNA, and 22% for samples containing a single copy. It is clear that multiple screens are required for detection in samples with such low copy numbers of target DNA, with the average cluster number representing the copy number in solution. To understand the tolerance of the cluster size criterion, the maps

DOI: 10.1021/jacs.6b02791
J. Am. Chem. Soc. 2016, 138, 7075−7081

were analyzed with different threshold values. When we selected 28.0 nm as the new cluster radius threshold, the same slope and adjusted R-squared value were observed, while the number of positive clusters in the map for samples containing five copies was slightly reduced, with an average value of 2.00, compared to 2.40 when a radius of 26.0 nm was used as the threshold (Figure S4 in the Supporting Information). This comparison demonstrates that setting an appropriate counting criterion with respect to cluster size is important; however, the results remain consistent within a range of cluster sizes (26.0−28.0 nm).

To assess the reliability of the detection efficiency, five adhesion maps were recorded for a single spot of captured target. When the maps were overlaid, the cluster was consistently placed at the same location in the probe DNA spot (Figure S5 in the Supporting Information). In addition, four clusters in a subsection of a spot were consistently observed at identical positions (Figure S6 in the Supporting Information). As an attempt to increase capture efficiency, we increased the hybridization time from 24 to 48 h; however, we observed that hybridization for 48 h did not increase the cluster number for a sample containing 24 copies of target DNA. Additionally, we examined the selectivity of the assay using a nontarget DNA (Figures S1 and S7 in the Supporting Information). While only five bases of the nontarget DNA matched with those of the probe DNA, it had a region complementary to the detection DNA for sensing. No cluster was observed on the probe spots when the spots were exposed to sample solutions of 100 aM (2.4×10^3 copies) or 10 fM (2.4×10^5 copies) of the nontarget DNA.

DISCUSSION

Advanced techniques using AFM for molecular recognition have been described;[20−22] however, the use of the hydrodynamic features of molecules captured on a surface to quantify the number of molecules per unit area has not previously been established. We observed that the hydrodynamic radius of the target DNA is a useful parameter for this purpose. Accurate localization of individual DNA molecules was achieved by overlapping a small number of adhesion force maps and applying appropriately chosen criteria to define positive clusters. In addition, repeated detection of a specific event within a pixel is a further criterion useful for discrimination of nonspecific and/or background pixels. All clusters obtained from the tested spots, including the samples listed in Table 1, were fitted into an ellipse for calculating the cluster radius (Figure 4b). While the most probable cluster radius was 32.6 ± 5.0 nm, larger clusters were detected during the analysis. Since we employed conventional speed atomic force microscopes, there were sizable drifts among the maps. Although we corrected for drift, imperfect correction may account for the majority of oversized clusters (five clusters with radii > 50.0 nm were observed among a total of 63 clusters). The oversized clusters were only counted once because fused clusters are only likely to be generated when a spot area is overcrowded. In addition, the shape of the clusters did not have a dumbbell appearance indicating double bindings.

A remarkable aspect of the current approach is the sensitivity of detection achieved. We attempted this method using spots generated with conventional microarrayers; however, the resulting spot size of hundreds of micrometers generated by these only allowed examination of a subsection of a spot at nanometer resolution using AFM, and the limit of detection is typically in the fM concentration range.[19,31] In this study, the miniaturized probe DNA spot (about two micrometers in diameter) enabled (1) the entire spot to be scanned by AFM, (2) the individual captured DNA target to be visualized, and (3) target DNA containing no more than 10 copies to be quantified. As the approach is direct, and does not require amplification, fluorophore labeling, or modification of target molecules, it will be useful in reducing uncertainty, particularly for samples where the target is present at very low abundance.

Precision and accuracy of the assay could be enhanced if variations in mapping, transport, capture efficiency, and sample preparation are minimized. Because the clusters were persistent when maps were generated consecutively on an identical spot (Figures S5 and S6 in the Supporting Information), it can be said that variation in mapping was low. Nevertheless, optimization of mapping parameters, including the pixel size and the number of repetitions, should further help increase reliability. Improving constant transport and capture efficiency is particularly important for assaying DNAs present at low copy number. Although the count number will be either zero or one for samples with a single copy, increasing the capture efficiency will reduce the number of repetitions required. Optimizing the hybridization and washing conditions and careful handing the sample (avoiding loss through nonspecific adsorption to the walls of pipets and glassware) would help attain both of these aims. Use of microfluidic devices would be an interesting option.[32] Because the samples were prepared through serial dilution steps, the copy number of some samples could be different from what was intended. However, this type of variation should be less problematic for clinical samples.

A major issue in the molecular monitoring of CML is the standard assessment of minimal residual disease (MRD), the minimal number of remaining leukemic cells capable of causing a relapse after treatment. The standard way to measure MRD relates the number of copies of *BCR-ABL* to those of control genes in the cell lysate. We observed that the probe DNA can discriminate the nontarget DNA up to 10^5 copies (Figure S7 in the Supporting Information). To be applicable to clinical samples, similar selectivity toward both *BCR* and *ABL* genes is needed, and this goal could be achieved by using more specific probes such as peptide nucleic acid (PNA) or locked nucleic acid (LNA).[33]

Together with enhanced AFM speed, there is a good chance that AFM could be adopted to the field of medical diagnostics, especially for samples in which targeted biomarkers cannot be amplified, or where the amplification process results in significant error. In addition, this approach should be useful for studying the equilibrium and dynamics of single molecules between solution and surface phases.

EXPERIMENTAL SECTION

Preparation of Target, Probe, and Detection DNAs. All DNAs were custom-synthesized (Integrated DNA Technologies Inc.). Target DNA (170-mer) consisted of sequences of the major *BCR-ABL* transcript (b2a2). Detection DNA (20-mer) is complementary to the *BCR* region of the target DNA.[34] Probe DNA (40-mer) was designed to recognize the translocated junction spanning the *BCR* (18-mer) and *ABL* (22-mer) regions. The detection and probe DNAs were functionalized with an amine group for immobilization on the AFM tip and substrate, respectively.

Preparation of Detection DNA Immobilized on an AFM Tip. Silicon nitride AFM tips (DPN Pen-Type B, Nanoink, Inc.) were coated with 27-acid dendrons, and an NHS group was generated at the apex of the dendrons using disuccinimidyl carbonate (Sigma-Aldrich),

DOI: 10.1021/jacs.6b02791
J. Am. Chem. Soc. 2016, 138, 7075−7081

as previously described.[35,36] The detection DNA (20 μM) was diluted in a buffer provided by NSB POSTECH, Inc., and AFM tips were dipped in the solution at room temperature for 12 h. To remove excess DNAs, tips were immersed in 2× SSC buffer (Sigma-Aldrich) containing 0.2% sodium dodecyl sulfate (pH 7.4) (Sigma-Aldrich) at 40 °C for 20 min, and washed with deionized water (18 MΩ·cm, Milli-Q purification system, Millipore). Tips with DNA attached were stored under vacuum (100 mTorr) until use.

Preparation of Etched Slides. Inductively coupled plasma (ICP) at the National Institute for Nanomaterials Technology (NINT, Korea) was employed to etch square boxes with a depth of 200 nm on each slide. Square boxes of 20 × 20 μm^2 were used for spotting. Patterned slides were coated with 27-acid dendrons by NSB POSTECH, Inc., and then treated with disuccinimidyl carbonate for activation.

Spotting Probe DNA onto Etched Slides. A cartridge kit (CytoClip, Cytosurge AG) with a premounted cantilever and a pyramidal tip with an aperture of 300 nm, was employed for dispensing probe DNA solution. The cantilever was 200 μm long and 36 μm wide, with a 1 μm internal channel, and a typical spring constant of 2 N/m. Probe DNA was diluted to 300 μM in 2× SSC buffer (pH 8.5) (Sigma-Aldrich), a concentration empirically chosen to inhibit clogging of the microchannel, while delivering sufficient probe DNA. Glycerol (Sigma-Aldrich) was added to the solution (final concentration, 12.5%) to adjust the evaporation rate. After injecting the solution (8 μL) into the reservoir, the cantilever was mounted on an atomic force microscope (FlexAFM, Nanosurf), and connected to a pressure controller (FluidFM microfluidics control system, Cytosurge AG). To fill the whole channel down to the tip opening with solution, the cantilever was brought into contact with the surface and an overpressure of +1000 mbar was applied for 30 s. The cantilever approached the sample surface with a specific set point of 200 mV. Two parameters, applied pressure to the channel and delay time after contacting the surface, were adjusted to control the droplet size. After spotting of the droplet, the slide was incubated in a humid chamber (80% humidity) at room temperature for 12 h. The slides were washed with 2× SSC buffer (Sigma-Aldrich) containing 0.2% sodium dodecyl sulfate (pH 7.4) (Sigma-Aldrich) at 40 °C for 20 min, and rinsed with deionized water (18 MΩ·cm, Milli-Q purification system, Millipore). The slides were then stored at 4 °C in a container filled with nitrogen.

Hybridization of Target DNA. Target DNA was serially diluted in 2× SSPE buffer (Sigma-Aldrich) containing 0.2% sodium dodecyl sulfate (pH 7.4), and samples containing 1.0 aM, 0.40 aM, 0.20, aM and 40 zM were prepared. A microarray hybridization kit (G2534A, Agilent Technologies) was used to incubate the target with the probe DNA spotted slide. We heated the solution containing the target DNA at 95 °C for 3 min, then loaded 40 μL into a chamber formed by a gasket. The slide was then placed into the kit, and the kit assembled. The assembled kit was placed in a rotator in a hybridization oven (Agilent Technologies) at 52 °C, and the spot on the slide was mixed effectively with the solution by rotation for 24 h. After disassembling the kit, the slide was washed with 0.2× SSPE buffer containing 0.02% sodium dodecyl sulfate (pH 7.4) for 20 min at 72 °C. After rinsing the slide with 0.2× SSC buffer (pH 7.4) at room temperature repeatedly, the slide was stored at 4 °C in PBS buffer (pH 7.4) (Sigma-Aldrich).

AFM Force Mapping. All force mapping experiments were performed using NanoWizard 1 and NanoWizard 3 atomic force microscopes (JPK Instrument). The spring constant of the AFM probes was calibrated using the thermal fluctuation method, with values between 0.03 and 0.04 N/m. All experiments were carried out in PBS buffer (pH 7.4) (Sigma-Aldrich) at room temperature. Extend and retract velocities were 3.0 μm/sec. The AFM tip was programmed to contact the surface with 80 pN, stay on the surface for 50 ms, then move a vertical distance of 200 nm. The adhesion force map of a single target DNA molecule was obtained within 120 × 120 nm^2 (15 × 15 pixels). FD curve-based images of a probe DNA spot consisted of 128 × 128 pixels (the maximum pixel numbers for NanoWizard 1), and the scan size (2.00 × 2.00 to 2.35 × 2.35 μm^2) was determined by the measured spot diameter.

FD Curve Analysis. For each adhesion force map (128 × 128 pixels) from a DNA spot, 16 384 FD curves were exported and processed by the JPK data processing program. Adhesion force and stretching distance values were measured by determination of the maximum value for each FD curve. Clustered pixels, indicating positive adhesion, were fitted to an ellipse using the "regionprops" function implemented in MATLAB, and the cluster radius was calculated.[25]

Overlay of Successively Obtained Force Maps. We created a program using MATLAB to calculate the degree of lateral drift between consecutively obtained force maps. Height and slope were converted to greyscale images, and each image was normalized by its mean intensity value. Two images were treated as two layers; the first one was fixed, while the other was moved pixel by pixel in x and y directions with respect to the fixed image. For each movement, the total value of the intensity difference in all pixels between the two maps was calculated, and the offset with the minimal difference provided the drift in x and y directions. To generate a final overlaid map, a third map was first overlaid onto the second map in the same way, and the combined map was then overlaid onto the first map.

■ ASSOCIATED CONTENT

Supporting Information

The Supporting Information is available free of charge on the ACS Publications website at DOI: 10.1021/jacs.6b02791.

Partial sequence of *BCR-ABL* gene; probe, detection and target DNA, and nontarget sequences used in the experiment; control experiment to test the reliability of the single molecule interaction between detection DNA immobilized on an AFM tip and target DNA captured on a probe DNA spot; schematic diagram of the simulated target DNA structure; calibration curve using a larger-cluster radius threshold; images generated from five consecutive maps (i) of the sample with a single copy of the target sequence and (ii) from a subsection of a spot; selectivity of the probe DNA (PDF)

■ AUTHOR INFORMATION

Corresponding Author

*jwpark@postech.ac.kr

Notes

The authors declare no competing financial interest.

■ ACKNOWLEDGMENTS

J.W.P. acknowledges the Brain Research Program (2015030964) of the National Research Foundation of Korea, and the R&D program of MSIP/COMPA (2015K000211) of Korea.

■ REFERENCES

(1) Gibson, U. E. M.; Heid, C. A.; Williams, P. M. *Genome Res.* **1996**, *6*, 995.

(2) Heid, C. A.; Stevens, J.; Livak, K. J.; Williams, P. M. *Genome Res.* **1996**, *6*, 986.

(3) VanGuilder, H. D.; Vrana, K. E.; Freeman, W. M. *BioTechniques* **2008**, *44*, 619.

(4) Hughes, T.; Janssen, J. W.; Morgan, G.; Martiat, P.; Saglio, G.; Pignon, J. M.; Pignatti, F. P.; Mills, K.; Keating, A.; Gluckman, E.; Bartram, C. R.; Goldman, J. M. *Lancet* **1990**, *335*, 1037.

(5) Gabert, J.; Beillard, E.; van der Velden, V. H. J.; Bi, W.; Grimwade, D.; Pallisgaard, N.; Barbany, G.; Cazzaniga, G.; Cayuela, J. M.; Cave, H.; Pane, F.; Aerts, J. L. E.; De Micheli, D.; Thirion, X.; Pradel, V.; Gonzalez, M.; Viehmann, S.; Malec, M.; Saglio, G.; van Dongen, J. J. M. *Leukemia* **2003**, *17*, 2318.

(6) Sanders, R.; Mason, D. J.; Foy, C. A.; Huggett, J. F. *Anal. Bioanal. Chem.* **2014**, *406*, 6471.

DOI: 10.1021/jacs.6b02791
J. Am. Chem. Soc. 2016, 138, 7075−7081

(7) Sykes, P. J.; Neoh, S. H.; Brisco, M. J.; Hughes, E.; Condon, J.; Morley, A. A. *Biotechniques* **1992**, *13*, 444.
(8) Kalinina, O.; Lebedeva, I.; Brown, J.; Silver, J. *Nucleic Acids Res.* **1997**, *25*, 1999.
(9) Vogelstein, B.; Kinzler, K. W. *Proc. Natl. Acad. Sci. U. S. A.* **1999**, *96*, 9236.
(10) Corbisier, P.; Pinheiro, L.; Mazoua, S.; Kortekaas, A. M.; Chung, P. Y. J.; Gerganova, T.; Roebben, G.; Emons, H.; Emslie, K. *Anal. Bioanal. Chem.* **2015**, *407*, 1831.
(11) McNally, B.; Singer, A.; Yu, Z.; Sun, Y.; Weng, Z.; Meller, A. *Nano Lett.* **2010**, *10*, 2237.
(12) Lee, H.; Park, J. E.; Nam, J. M. *Nat. Commun.* **2014**, *5*, 3367.
(13) Cai, H.; Parks, J. W.; Wall, T. A.; Stott, M. A.; Stambaugh, A.; Alfson, K.; Griffiths, A.; Mathies, R. A.; Carrion, R.; Patterson, J. L.; Hawkins, A. R.; Schmidt, H. *Sci. Rep.* **2015**, *5*, 14494.
(14) Lee, G. U.; Chrisey, L. A.; Colton, R. J. *Science* **1994**, *266*, 771.
(15) Strunz, T.; Oroszlan, K.; Schafer, R.; Guntherodt, H. J. *Proc. Natl. Acad. Sci. U. S. A.* **1999**, *96*, 11277.
(16) Kufer, S. K.; Puchner, E. M.; Gumpp, H.; Liedl, T.; Gaub, H. E. *Science* **2008**, *319*, 594.
(17) Dufrene, Y. F.; Martinez-Martin, D.; Medalsy, I.; Alsteens, D.; Muller, D. J. *Nat. Methods* **2013**, *10*, 847.
(18) Jung, Y. J.; Albrecht, J. A.; Kwak, J. W.; Park, J. W. *Nucleic Acids Res.* **2012**, *40*, 11728.
(19) Iyer, S.; Gaikwad, R. M.; Subba-Rao, V.; Woodworth, C. D.; Sokolov, I. *Nat. Nanotechnol.* **2009**, *4*, 389.
(20) Ebner, A.; Kienberger, F.; Kada, G.; Stroh, C. M.; Geretschlager, M.; Kamruzzahan, A. S. M.; Wildling, L.; Johnson, W. T.; Ashcroft, B.; Nelson, J.; Lindsay, S. M.; Gruber, H. J.; Hinterdorfer, P. *ChemPhysChem* **2005**, *6*, 897.
(21) Husale, S.; Persson, H. H. J.; Sahin, O. *Nature* **2009**, *462*, 1075.
(22) Pfreundschuh, M.; Alsteens, D.; Wieneke, R.; Zhang, C.; Coughlin, S. R.; Tampe, R.; Kobilka, B. K.; Muller, D. J. *Nat. Commun.* **2015**, *6*, 8857.
(23) de Klein, A.; van Kessel, A. G.; Grosveld, G.; Bartram, C. R.; Hagemeijer, A.; Bootsma, D.; Spurr, N. K.; Heisterkamp, N.; Groffen, J.; Stephenson, J. R. *Nature* **1982**, *300*, 765.
(24) Yee, K.; Anglin, P.; Keating, A. *Blood Rev.* **1999**, *13*, 105.
(25) Lee, Y.; Kwon, S. H.; Kim, Y.; Lee, J. B.; Park, J. W. *Anal. Chem.* **2013**, *85*, 4045.
(26) Saenger, W. *Principles of nucleic acid structure*; Springer-Verlag: New York, 1984.
(27) Haasnoot, C. A.; de Bruin, S. H.; Berendsen, R. G.; Janssen, H. G.; Binnendijk, T. J.; Hilbers, C. W.; van der Marel, G. A.; van Boom, J. H. *J. Biomol. Struct. Dyn.* **1983**, *1*, 115.
(28) Hilbers, C. W.; Haasnoot, C. A.; de Bruin, S. H.; Joordens, J. J.; van der Marel, G. A.; van Boom, J. H. *Biochimie* **1985**, *67*, 685.
(29) Baumann, C. G.; Smith, S. B.; Bloomfield, V. A.; Bustamante, C. *Proc. Natl. Acad. Sci. U. S. A.* **1997**, *94*, 6185.
(30) Gruter, R. R.; Voros, J.; Zambelli, T. *Nanoscale* **2013**, *5*, 1097.
(31) Roy, D.; Kwon, S. H.; Kwak, J. W.; Park, J. W. *Anal. Chem.* **2010**, *82*, 5189.
(32) Yuen, P. K.; Li, G.; Bao, Y.; Muller, U. R. *Lab Chip* **2003**, *3*, 46.
(33) Mishra, S.; Lahiri, H.; Banerjee, S.; Mukhopadhyay, R. *Nucleic Acids Res.* **2016**, *44*, 3739.
(34) Goh, H. G.; Hwang, J. Y.; Kim, S. H.; Lee, Y. H.; Kim, Y. L.; Kim, D. W. *Transl. Res.* **2006**, *148*, 249.
(35) Jung, Y. J.; Hong, B. J.; Zhang, W.; Tendler, S. J. B.; Williams, P. M.; Allen, S.; Park, J. W. *J. Am. Chem. Soc.* **2007**, *129*, 9349.
(36) Roy, D.; Park, J. W. *J. Mater. Chem. B* **2015**, *3*, 5135.

DOI: 10.1021/jacs.6b02791
J. Am. Chem. Soc. 2016, 138, 7075−7081